



Contents lists available at ScienceDirect

# Methods

journal homepage: [www.elsevier.com/locate/ymeth](http://www.elsevier.com/locate/ymeth)



## Millisecond phase kinetic analysis of elongation catalyzed by human, yeast, and *Escherichia coli* RNA polymerase

Maria Kireeva<sup>a</sup>, Yuri A. Nedialkov<sup>a,b,1</sup>, Xue Qian Gong<sup>b,2</sup>, Chunfen Zhang<sup>b,3</sup>, Yalin Xiong<sup>b,4</sup>, Woo Moon<sup>b</sup>, Zachary F. Burton<sup>b,\*</sup>, Mikhail Kashlev<sup>a</sup>

<sup>a</sup>Gene Regulation and Chromosome Biology Laboratory, National Cancer Institute—Frederick, Bldg. 539, Room 222, Frederick, MD 21702-1201, USA

<sup>b</sup>Department of Biochemistry and Molecular Biology, Michigan State University, E. Lansing, MI 48824-1319, USA

### ARTICLE INFO

Article history:  
Accepted 6 April 2009  
Available online xxxxx

Keywords:  
Rapid chemical quench flow  
Pre-steady state kinetic analysis  
Elongation  
RNA polymerase II  
RNA polymerase  
Elongation factors  
Ternary elongation complex  
Transient state inhibition  
 $\alpha$ -Amanitin

### ABSTRACT

Strategies for assembly and analysis of human, yeast, and bacterial RNA polymerase elongation complexes are described, and methods are shown for millisecond phase kinetic analyses of elongation using rapid chemical quench flow. Human, yeast, and bacterial RNA polymerases function very similarly in NTP-Mg<sup>2+</sup> commitment and phosphodiester bond formation. A “running start, two-bond, double-quench” protocol is described and its advantages discussed. These studies provide information about stable NTP-Mg<sup>2+</sup> loading, phosphodiester bond synthesis, the processive transition between bonds, and sequence-specific effects on transcription elongation dynamics.

© 2009 Published by Elsevier Inc.

### 1. Introduction

Methods to analyze the kinetics of elongation catalyzed by multi-subunit RNA polymerases (RNAPs) have included single molecule and ensemble methods. Such approaches are complementary for understanding elongation, and each method has potential advantages and limitations. Single molecule approaches [1] allow behavior of individual molecules to be tracked, but these methods are often not easily amenable to parallel analyses of many samples, and there remain technical limitations to resolving details of single bond synthesis. Ensemble approaches average the behavior of many molecules, potentially obscuring individual characteristics but allowing analysis of many samples and experimental conditions (i.e., presence or absence of inhibitors and/or elongation factors, different pH, alternate divalent cation, etc.). Rapid chemical

quench flow is an ensemble approach that provides significant insight into individual phosphodiester bond additions [2–13].

The majority of DNA polymerases bind somewhat loosely to a template-primer [14]. Because of reversible binding, much higher amounts of a DNA polymerase may be required for pre-steady state kinetic analysis, and dissociation and association rates must be considered in quantifying elongation kinetics. By contrast, multi-subunit RNAPs are highly processive, meaning that ternary elongation complexes (TECs) do not easily dissociate, and the high processivity of RNAPs has been exploited in the kinetic analysis of elongation. Because RNAPs tenaciously retain their templates, very small quantities of a TEC can be monitored using radioisotope detection (i.e., low femtomole quantities of TEC are sufficient per data point). In general, the goal of pre-steady state kinetic experiments is to reveal information about the central core of an enzyme mechanism, rather than the ultimate exchange of substrates and products, which can be addressed using steady state kinetic methods [15].

In this paper, we describe approaches for pre-steady state kinetic analyses of elongation catalyzed by human – *Homo sapiens* (H.s.) and *Saccharomyces cerevisiae* (S.c.) RNA polymerase II (Pol II), and *Escherichia coli* (E.c.) RNA polymerase (RNAP). The method, which utilizes rapid chemical quench flow technology and multiple reaction quenching strategies, is rapid and flexible and can be applied to many samples. Significant information is obtained about

\* Corresponding author. Fax: +1 517 353 9334.

E-mail address: [burton@msu.edu](mailto:burton@msu.edu) (Z.F. Burton).

<sup>1</sup> Present address: Department of Biochemistry, New York University, NY 10016, USA.

<sup>2</sup> Present address: Lilly Research Laboratories, Greenfield, IN 46140, USA.

<sup>3</sup> Present address: Hematology Division, Washington University School of Medicine, St. Louis, MO 63110, USA.

<sup>4</sup> Present address: University of Washington, VM Bloedel Hearing Research Center, Box 357923, Seattle, WA 98195-7923, USA.

pausing, escape from a transcriptional stall, and rate-limiting steps during elongation, including stable NTP-Mg<sup>2+</sup> loading, phosphodiester bond formation, and the processive transition between formation of one bond and the next (generally, the interval between phosphodiester bond formation and the next stable NTP-Mg<sup>2+</sup> loading).

## 2. Instrumentation

The method of rapid chemical quench flow allows rapid reaction starts and stops, so that millisecond (ms) reaction times are possible [15]. The ms phase is an appropriate timescale for analysis of elongation because rate-limiting steps ( $k \sim 25 \text{ s}^{-1}$ ) and some faster steps ( $k > 100 \text{ s}^{-1}$ ) during RNA synthesis can be observed using ms time resolution. The protocols shown here were done with the KinTek RQF-3 (3-syringe) and RQF-4 (4-syringe) rapid chemical quench flow instruments, which are capable of starting and stopping a reaction within 2-ms. Quench flow differs from stop flow fluorescence approaches in that one need not consider a “dead time” lag in kinetic measurements using quench flow. If the instrument is properly calibrated, a 2-ms time point can be obtained with high reproducibility, accuracy and precision.

The RQF-3 and RQF-4 instruments have some advantages and some limitations. One advantage of the KinTek instrument is the use of small sample loops (15  $\mu\text{l}$  sample volume). We find that the data obtained using the KinTek instruments can be highly reproducible, even when experiments are done months apart or before and after instrument calibration. A potential limitation of the technology is that it is not very flexible in terms of experimental design. The 3-syringe RQF-3 instrument is designed primarily for rapid reaction starts and stops, and is limited in its use for more complex reaction designs, involving multiple reagent additions. The four syringe RQF-4 instrument allows two reagent additions before quenching, with about a minimum 10-ms timing on the initial addition followed by a minimum 2-ms timing on the final addition. The only significant drawback of the RQF-4 is the requirement for a noticeably larger volume of the substrate solution per experiment than for the RQF-3 (approximately 130 and 20  $\mu\text{l}$ , respectively, per sample). To reduce the consumption of expensive ultra-pure NTPs (Amersham) in pre-steady state experiments using the RQF-4, we use NTP stocks reconstituted from powdered NTPs (Sigma) as the reaction substrate. The powdered NTPs are dissolved in water to achieve 100 mM concentration, the pH of the solution is adjusted to 7.0 with NaOH or LiOH, and the final substrate solution is prepared by diluting the stock NTP with transcription buffer. Note that powdered NTPs contain detectable amounts of all four NTPs, and only the ultra-pure NTPs (Amersham) should be used for the running start reaction or for substrate misincorporation assays.

## 3. Strategies and system characterization

### 3.1. Running start, two-bond, double-quench (RTD) protocol

The method developed for the pre-steady-state kinetic analyses of H.s. Pol II has been described as the “running start, two-bond, double-quench” (RTD) protocol [8,10,11]. An essential part of this analysis is the use of two quenching strategies, which provide distinct information about RNAP dynamics. Proposed mechanisms for E.c. RNAP and H.s. Pol II so far have relied on incomplete data sets or, in some cases, too much reliance has been placed on a single quenching strategy [2,8,16]. Sole reliance, for instance, on data from EDTA quenching gives an ambiguous picture of the RNAP mechanism, which is significantly simplified by inclusion of HCl

quench data. For an adequate kinetic analysis, it is also essential to monitor the synthesis of at least two bonds.

#### 3.1.1. Running start

It has been shown that RNAPs undergo slow catalytic inactivation upon stalling at some template positions [17–20]. A switch to a slowly elongating or arrested conformation of RNAP upon prolonged substrate deprivation was detected for both bacterial RNAP and eukaryotic Pol II, and a slow escape of RNAP from these off-pathway states made precise measurement of the rates of subsequent bond formation challenging [8,9,20] (see Fig. 1; bottom right plot). The idea of a “running start” was introduced in order to minimize TEC inactivation. In this method, the TEC stalled at a unique position was advanced for a defined, brief time (i.e., 1–30 s; the RQF-4 can be used for a 1–10 s NTP addition; a 30 s addition can be done on the bench top, with a subsequent loading of the TEC into the sample port of the RQF-3), using one or two NTP substrates. In the experiment shown in Fig. 1, H.s. Pol II is advanced by a 30 s running start from C40 to A43, by addition of ATP. In many instances, the running start was found necessary to obtain reproducible elongation kinetics and consistent distributions of paused and active pathway TECs (for example, see Fig. 8 below).

#### 3.1.2. Tracking two consecutive bonds

Transcription is highly processive and RNAP translocates along DNA by single base increments without dissociation, in order to form the next phosphodiester bond. The processive transition is the interval between formation of one phosphodiester bond and stable NTP-Mg<sup>2+</sup> loading for the next bond synthesis. Translocation is concomitant with release of inorganic pyrophosphate as the byproduct of the previous bond formation. During the processive transition, translocation and/or pyrophosphate release can in principle limit the overall elongation rate of the enzyme. Therefore, in order to ensure that at least one processive transition is observed, at least two bonds must be tracked. For H.s. and S.c. Pol II, as well as for bacterial RNAP, the processive transition appears to include a rate-limiting and NTP-dependent step, so monitoring two bonds is minimally essential. In addition to translocation and pyrophosphate release, a conformational change in the TEC is also likely during the processive transition. In Fig. 1, GTP is added to support both G44 and G45 synthesis, ensuring that the processive transition between the G44 and the G45 bond formation is observed. Still another way to consider the importance of monitoring (at least) two bonds is to realize that escape of Pol II from a stall position may not be identical to ongoing processive RNA synthesis, because rate-limiting steps in elongation may be bypassed during the stall.

#### 3.1.3. EDTA/HCl quenching and pulse-chase protocols

EDTA/HCl quenching and pulse-chase protocols are used because different kinetics is observed depending on the reagent that is used to stop the reaction (Fig. 1); so different quenching agents provide distinct information. Stopping the reaction with 1 M HCl, which instantly inactivates RNAP, identifies the kinetics of phosphodiester bond formation [4,10,11,13,21,22]. Stopping the reaction with 0.5 M EDTA, on the other hand, identifies the timing of stable NTP-Mg<sup>2+</sup> loading, which, interestingly, for H.s. and S.c. Pol II and E.c. RNAP is not initially coincident with phosphodiester bond formation [7,11,13,22]. EDTA is known to be a high affinity Mg<sup>2+</sup> chelation agent, so EDTA quenches the reaction by depleting Mg<sup>2+</sup> ions, unless they are sequestered within the enzyme in the NTP-Mg<sup>2+</sup> complex. The NTP is shown to be sequestered along with the Mg<sup>2+</sup>, because quenching the reaction with an excess of unlabeled NTP instead of EDTA allows S.c. Pol II to complete incorporation of a labeled NTP substrate, despite the addition of excess unlabeled substrate [7]. We conclude from this analysis that EDTA

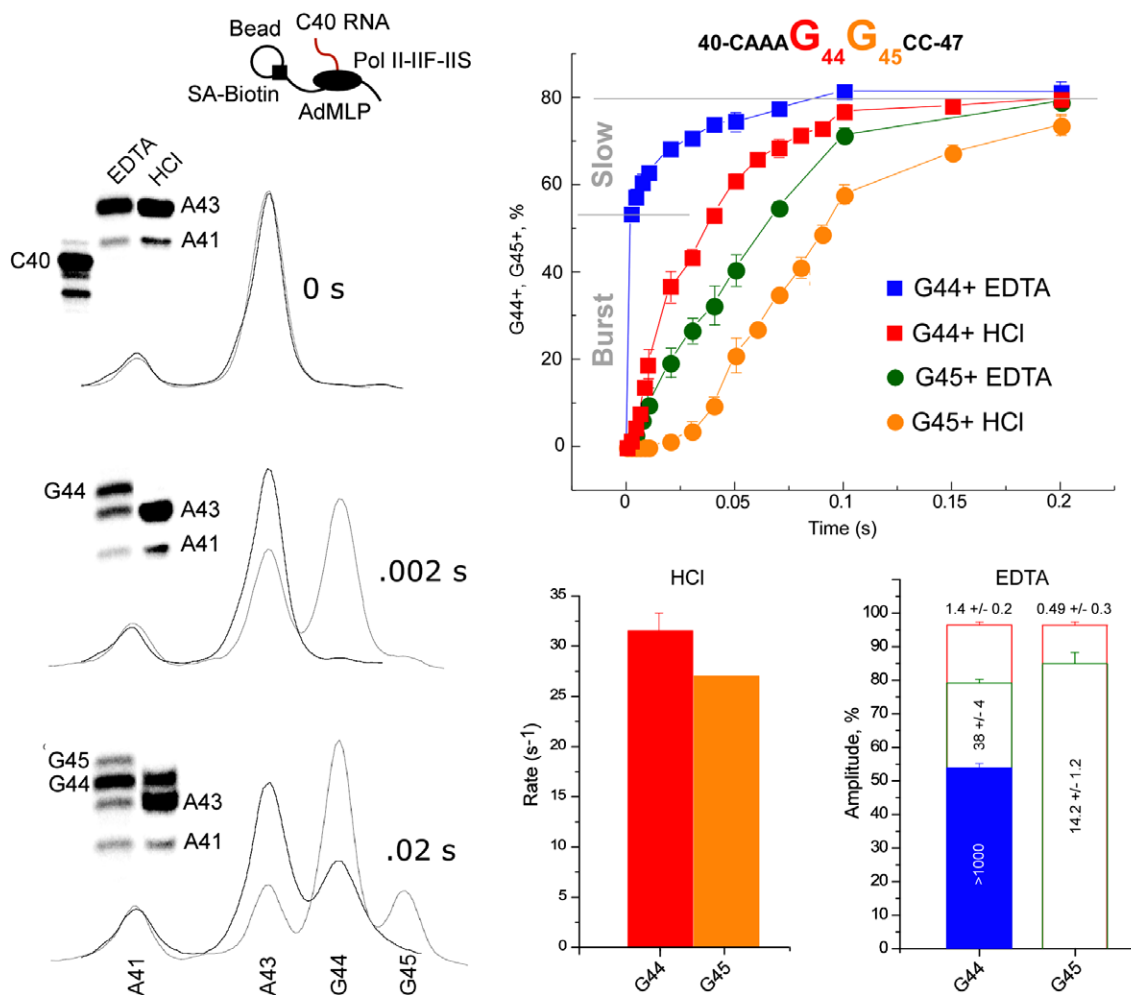


**Fig. 1.** Elongation dynamics of promoter-initiated H.s. Pol II TECs in the presence of TFIIF and TFIIS. The RTD protocol and sequence for RNA synthesis through the G44 and G45 positions are indicated at the top of the figure. The source of transcription factors was an extract of HeLa nuclei. C40 TECs were initiated, from bead-immobilized templates (SA indicates streptavidin) containing the Adenovirus major late promoter and a modified downstream sequence, with dATP, ApC dinucleotide, <sup>32</sup>P-CTP and UTP and washed [8]. For the running start to A43, ATP was added for 30 s. In the KinTek RQF-3, reactions were started by addition of GTP and quenched with EDTA or HCl, as indicated in the key (top plot). G44+ indicates G44 plus all longer transcripts (the G44 synthesis rate neglecting G44 disappearance with elongation to longer positions). Times are in seconds (s). Selected gel data and densitometric scans (arbitrary units) are shown at the left of the figure. Black lines indicate HCl quench; gray lines indicate EDTA quench. In the plot, data are shown to 0.2 s. Error bars in the top plot indicate standard deviation of at least three independent experiments. Some error bars are obscured by graph symbols. Apparent rates of phosphodiester bond synthesis from HCl quenching are compared (lower left plot). The rate reported for G45 synthesis (orange bar) is the rise rate after fitting the 25-ms lag in G45 appearance. Amplitudes for multiple phase exponential curve fits (corresponding to fractions of the TEC) are shown in the right bottom plots for EDTA quench data, along with associated rates (s<sup>-1</sup>). Errors and error bars indicate standard error from exponential curve fitting. Data are reproduced from Zhang et al. (2004) with permission [11]. Colors and plots are consistent with Figs. 3-7.

197 quenches free NTP-Mg<sup>2+</sup> but does not quench protected NTP-  
198 Mg<sup>2+</sup>, presumably sequestered within the Pol II active site. At early  
199 times, less incorporation is observed with HCl quenching, showing  
200 that NTP-Mg<sup>2+</sup> is sequestered (pulse-chase or EDTA quench) but  
201 the phosphodiester bond has not yet formed (HCl quench). Others,  
202 studying DNA polymerase or single subunit RNAP elongation, have  
203 interpreted HCl, EDTA, and unlabeled NTP quench (pulse-chase)  
204 data in very similar ways [22].

### 205 3.1.4. An example of the RTD Protocol

206 An example of the RTD method is shown in Fig. 1 (reproduced  
207 from [11]). H.s. C40 Pol II TECs (<sup>32</sup>P-labeled 40 nucleotide RNAs  
208 ending in 3'-CMP) are prepared by accurate initiation from the  
209 adenovirus major late promoter. The sequence downstream of  
210 the promoter was modified so that a 40-mer RNA could be syn-  
211 thesized with ApC dinucleotide, CTP (α<sup>32</sup>P-labeled), and UTP. <sup>32</sup>P-  
212 C40 TECs were extended to A43 by a 30-s incubation with  
213 100 μM ATP (running start). Using the KinTek RQF-3 rapid chem-

214 ical quench flow instrument, 2.5 mM GTP was added, and reac-  
215 tions were stopped by HCl or EDTA quenching (Fig. 1).  
216 Synthesis of G44 and G45 was monitored and is reported as  
217 G44 or G45 plus all longer transcripts (G44+ and G45+). Samples  
218 were done in triplicate (at least three independent experiments  
219 done on different days), and error bars indicate standard deviation  
220 (top plot). Because 2.5 mM GTP is well above the apparent  
221 K<sub>d</sub> for GTP binding (K<sub>d</sub> = 16 μM), the reaction is run near maximal  
222 velocity, providing detailed insight into different detectable reac-  
223 tion rates that do not depend on limiting NTP concentration. HCl  
224 quenching provides the timing of phosphodiester bond addition  
225 for G44 and G45 synthesis. EDTA quench curves do not coincide  
226 with HCl quench curves, so EDTA quenching provides different  
227 information about reaction progression. Because stable GTP-  
228 Mg<sup>2+</sup> sequestration (EDTA quench) occurs prior to bond forma-  
229 tion (HCl quench), GTP-Mg<sup>2+</sup> can be sequestered, presumably  
230 within the Pol II active site, prior to formation of the G44 phos-  
231 phosphodiester bond.

Model independent analysis of EDTA and HCl quench data provides further insight. In this case, elongation rates to 5 s (full curves are not shown) were fit using the simplest exponential curves (single, double, or triple exponentials) to adequately fit the data. The apparent rates ( $k_{app}$  in units of  $s^{-1}$ ) and associated amplitudes (corresponding to the percent of TECs associated with a particular rate) are indicated. The bottom left panel shows the apparent rates of HCl quench data. The bottom right panel indicates the amplitudes and associated rates for EDTA quench data from triple or double exponential curve fits. All C40 TECs advance within 30 s (data not shown).

Interestingly, a burst is observed in GTP-Mg<sup>2+</sup> sequestration that is too fast to accurately measure using rapid chemical quench flow ( $k$  is faster than  $1000 s^{-1}$ ). This result means that GTP-Mg<sup>2+</sup> loading ( $k_{app} > 1000 s^{-1}$ ) for H.s. Pol II is not rate-limiting ( $k \sim 15\text{--}25 s^{-1}$  at 25 °C). The secondary pore of H.s. Pol II is a solvent-accessible route to the active site. Based on negative pore electrostatics, Kornberg and colleagues predicted that NTP loading for S.c. Pol II through the secondary pore must be rate-limiting for elongation [23], but NTP loading is not rate limiting for H.s. Pol II. This is one reason to question whether NTPs load primarily or solely through the secondary pore.

In the rapid quench flow analysis, two rate-limiting steps in RNA synthesis are observed. One rate-limiting step is identified between stable GTP-Mg<sup>2+</sup> binding and phosphodiester bond formation: the interval between an EDTA quench curve and the HCl quench curve. Thus, phosphodiester bond formation or an associated conformational change appears to be rate-limiting, after rapid and stable GTP-Mg<sup>2+</sup> acquisition. Another rate-limiting step is identified between phosphodiester bond formation and the next stable GTP-Mg<sup>2+</sup> loading: the interval between the HCl quench curve for G44 synthesis and the EDTA quench curve for G45 synthesis. This interval is referred to as the processive transition and this step includes: (1) pyrophosphate release; (2) translocation; and (3) stable GTP-Mg<sup>2+</sup> loading (which appears to be rapid (see above)). We conclude that for formation of the two consecutive bonds with GTP there are two rate-limiting steps during each bond and that these steps occur within intervals defined by the EDTA and HCl quench procedures.

Fig. 1 shows that the processive transition is rate-limiting for H.s. Pol II. Although the rise rate is similar for G45 synthesis compared to the rate of G44 synthesis (orange and red bars in the bottom left plot), there is a 25-ms lag in the first appearance of G45 (compare the red and orange curves in the top plot). This lag provides evidence of a rate-limiting step during the processive transition between G44 and G45 phosphodiester bond synthesis, from HCl quench data. Because the rise rate for G45 synthesis is not much slower than the rate for G44 synthesis, formation of the G45 bond is not in itself a slow step in the mechanism (see below). Comparing the synthesis of the G44 bond ( $k_{app} = 31.6 \pm 1.7 s^{-1}$ ; amplitude  $80.1 \pm 1.4\%$  of TECs (not shown); HCl quench) and stable GTP-Mg<sup>2+</sup> loading for G45 synthesis ( $k_{app} = 14.2 \pm 1.2 s^{-1}$ ; amplitude  $85.4 \pm 3.2\%$  of TECs; EDTA quench), it is clear that a rate-limiting step has occurred in the processive interval. As we show below, kinetics of elongation catalyzed by S.c. Pol II and E.c. RNAP are very similar to H.s. Pol II.

### 3.2. Elongation factors

The human system is useful for the analysis of factors that interact directly with the TEC to stimulate elongation [3,4,8,10–12]. H.s. transcription factor IIF (TFIIF) binds to H.s. Pol II and strongly stimulates elongation rates. TFIIS has not been reported to stimulate elongation rate, but, rather, overcomes blocks to transcription through stimulation of a TFIIS- and Pol II-dependent endonuclease cleavage near the 3'-end of the nascent RNA. TFIIS, therefore, exerts

its greatest effects on the pausing and backtracking pathways rather than the rapid elongation pathway. TFIIF and TFIIS have been analyzed for their effects on the elongation mechanism using quench flow. TFIIF accelerates phosphodiester bond synthesis and the processive transition between bonds. TFIIF can be thought of as an allosteric effector of Pol II elongation, accelerating rate-limiting steps in the mechanism: bond formation and the processive transition. TFIIS affects the distribution of TECs at a stall position and stimulates intrinsic cleavage of a dinucleotide from the RNA 3'-end.

Hepatitis delta antigen is the sole gene product encoded by hepatitis delta virus, a small RNA genome viroid satellite transmitted by hepatitis B virus infection [24–26]. Hepatitis delta antigen stimulates the ribozyme activity necessary for monomerization and cyclization of the hepatitis delta virus RNA genome. Hepatitis delta antigen is thought to stimulate H.s. Pol II to transcribe and replicate the hepatitis delta virus RNA, converting H.s. Pol II from a DNA-dependent to an RNA-dependent RNAP. Similar to TFIIF, using DNA templates for transcription, hepatitis delta antigen accelerates the rates of phosphodiester bond synthesis and the processive transition between bonds. Hepatitis delta antigen appears to interact with the Pol II mobile clamp, which holds the RNA–DNA hybrid, to stimulate elongation.

### 3.3. Using $\alpha$ -amanitin as a transient state inhibitor of H.s. Pol II

#### 3.3.1. $\alpha$ -Amanitin reveals the existence of two distinct conformations of Pol II in active TECs

The mushroom toxin  $\alpha$ -amanitin binds in the vicinity of the active center of Pol II but does not directly interfere with catalytic function [27–29]. This drug has been used in the Burton laboratory to probe the mechanism of phosphodiester bond formation catalyzed by H.s. Pol II [3,4,10]. Because elongation is very slow for TECs that are pre-incubated with  $\alpha$ -amanitin [30,31], a protocol was designed in which the drug was added at a higher concentration at (or close to) the time of NTP addition. Using this approach, it was found that a large fraction of TECs, apparently equal in amplitude to the 2-ms EDTA burst fraction of Fig. 1 [3,4,10], was initially resistant to inhibition, as if these TECs were in a conformation that did not bind or resisted inhibition by the toxin. Resistant H.s. Pol II TECs become strongly sensitive to  $\alpha$ -amanitin before addition of a second bond, indicating that resistant and sensitive conformations of the TEC occur in each (or most) bond addition cycles [3,4,10].

#### 3.3.2. $\alpha$ -Amanitin used as a transient state inhibitor reveals downstream NTP effects

In Fig. 2, an experiment is shown (reproduced from [10]) in which  $\alpha$ -amanitin and NTPs are added simultaneously to a H.s. Pol II A43 TEC, using an RTD protocol from C40. This experiment shows unexpected effects of  $\alpha$ -amanitin and downstream CTP and UTP on stable GTP-Mg<sup>2+</sup> commitment, G44 phosphodiester bond formation and G44 bond completion. 2.5 mM GTP was added together with 0.5 mM  $\alpha$ -amanitin. To test for possible effects of downstream NTPs, 0.5 mM CTP and UTP were added or omitted, as indicated. Reactions were quenched with EDTA or HCl. In the presence of  $\alpha$ -amanitin, CTP and/or UTP induce reversal of stable GTP-Mg<sup>2+</sup> binding and G44 phosphodiester bond synthesis. Control experiments show that CTP is essential and UTP is stimulatory to enhance reversal activities [10]. We conclude the following from this experiment: (1) a fraction of A43 TECs is resistant to  $\alpha$ -amanitin inhibition (apparently equal to the fraction observed in the EDTA quench burst); (2) CTP and/or UTP alter GTP-Mg<sup>2+</sup> commitment (EDTA quench) and G44 bond synthesis (HCl quench); and (3)  $\alpha$ -amanitin appears to block G44 bond completion (pyrophosphate release). Because CTP and UTP are templated at downstream positions ( $i + 2/j + 3/i + 4$ ) and GTP-Mg<sup>2+</sup> or GMP.PPi (GMP complexed to pyrophosphate in  $i + 1$ ) occupies the

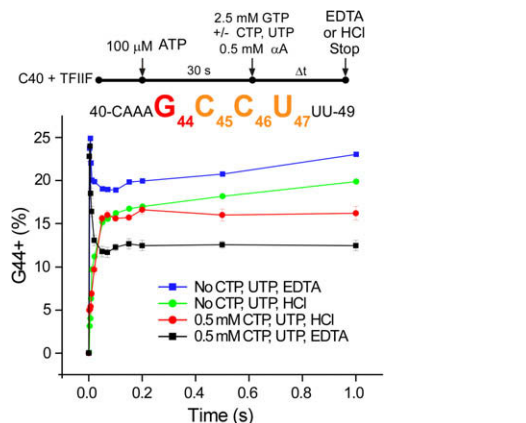


**Fig. 2.** Transient state inhibition of the H.s. Pol II TEC by the mushroom toxin  $\alpha$ -amanitin and evidence for pre-loading of NTP substrates. The protocol and RNA sequence are shown at the top of the figure. Addition of CTP and UTP (templated at the  $i + 2$ ,  $i + 3$ , and  $i + 4$  downstream positions) affects isomerization and incorporation of GMP at the G44 ( $i + 1$ ) position. Error bars indicate standard deviation of at least three independent experiments. The figure is reproduced from Xiong and Burton, with permission [10]; confirming experiments and additional controls are shown in that paper. The failure of EDTA quench and HCl quench curves to converge before 1 s indicates that G44 phosphodiester bonds are formed (HCl quench) but not completed (EDTA quench): pyrophosphate release is not complete.

active site, we take the effects of CTP and UTP on G44 synthesis as an indication of pre-loading of NTP substrates to downstream template positions.

### 3.3.3. Failure of EDTA and HCl quench curves to converge indicates that G44 bonds may be formed but not completed

Convergence of EDTA quench (GTP-Mg<sup>2+</sup> commitment) and HCl quench (G44 bond formation) curves, as observed in Fig. 1, is expected at later reaction times [10]. In Fig. 2, EDTA and HCl quench curves fail to converge within 1 s, indicating that formation of the G44 bond is not fully resolved. This unexpected result is an indication that, in the presence of  $\alpha$ -amanitin, G44 bond completion is blocked. We suggest that formation of the G44 phosphodiester bond remains reversible because pyrophosphate is retained in the Pol II active site after bond formation (as GMP.PPi). In the EDTA quench experiment, in the presence of CTP and UTP, G44 bonds that were formed at the time of EDTA quench addition are reversed prior to system equilibration because of EDTA-depletion of CTP- and UTP-Mg<sup>2+</sup> interacting at downstream template sites [10].

It is clear from previously published experiments with  $\alpha$ -amanitin that the toxin inhibits the processive transition between bonds [3,4,10]. The Burton laboratory proposed that  $\alpha$ -amanitin blocked H.s. Pol II translocation, but, according to current information, this may not be the best description. The toxin, for instance, could block another step in the processive interval, such as: (1) pyrophosphate release; (2) reverse isomerization of the TEC (a conformational change); or (3) stable CTP-Mg<sup>2+</sup> loading. However, because GTP-Mg<sup>2+</sup> loading was not blocked for G44 bond formation at the A43 stall position (Fig. 2), CTP-Mg<sup>2+</sup> loading for C45 synthesis is unlikely to be the target of  $\alpha$ -amanitin inhibition. Most likely,  $\alpha$ -amanitin blocks a necessary conformational change during the processive transition. A recent crystal structure indicated that  $\alpha$ -amanitin might stabilize a post-translocated TEC with the  $i + 1$  template DNA base rotated out of the active site [27]. The “trigger loop” of Pol II is a mobile element of the Rpb1 subunit that, in its closed conformation, locks the NTP-Mg<sup>2+</sup> in the active site during phosphodiester bond formation. From structures,  $\alpha$ -amanitin is proposed to require an open conformation of the trigger loop and specific interactions with S.c. Rpb1 H1085, located on the trigger loop, for stable toxin binding [27–29]. Because a closed trigger

helices structure is expected to support G44 bond formation, perhaps the trigger loop must relax for  $\alpha$ -amanitin to bind and inhibit C45 synthesis. Such a conformational change could be an element of the processive transition.

Experiments with  $\alpha$ -amanitin appear to fulfill a major goal of halting H.s. Pol II, using a powerful inhibitor, in the core of the elongation mechanism [10]. A major focus of pre-steady state kinetic experiments is to reveal the internal mechanism of an enzyme, in this case, H.s. Pol II, frozen in the act of synthesis. In this protocol,  $\alpha$ -amanitin is used as a transient state inhibitor of RNA synthesis, establishing a rapid block to forward chain extension. To our knowledge, ours was the first report of successful transient state inhibition of an RNAP reaction [10]. Downstream NTPs affect previous bond formation, demonstrating the major tenet of the NTP-driven translocation mechanism: that NTPs bind to downstream template DNA sites and affect previous bond formation [10]. Another major tenet of the NTP-driven translocation mechanism is that pyrophosphate release is coupled to the next accurate NTP loading, an observation recently reported by Johnson et al. studying elongation catalyzed by E.c. RNAP [32].

### 3.4. Experiments with S.c. Pol II and E.c. RNAP

A major motivation for developing a system for pre-steady state analysis of elongation catalyzed by S.c. Pol II and E.c. RNAP is to make use of the large number of available mutants with defects in elongation [7]. In principle, analysis of these mutant proteins can provide insight into which steps in elongation are affected by particular mutations in order to gain insight into atomic details of RNAP structure–function and dynamics. A detailed study of S.c. Pol II Rpb1 E1103G and E1103A mutations was recently reported indicating the power of this approach [7]. E1103G is error-prone and sequesters NTP-Mg<sup>2+</sup> more efficiently than wild type Pol II without a dramatic effect on the rate of phosphodiester bond formation. Detailed quench flow analyses have also been reported for site-directed mutations in E.c. RNAP [6].

Promoter-based initiation cannot as easily be used to analyze S.c. Pol II, because the yeast enzyme utilizes a different mechanism than H.s. Pol II for selecting a transcriptional start site. Yeast enzyme scans from a promoter DNA sequence (i.e., a TATA box) 70 to 100 nucleotides downstream to initiate transcription, which may occur at multiple sites. Because of this difference in start site selection, it is challenging to synthesize RNA with a defined length from a S.c. Pol II promoter. An alternate strategy, and one with additional potential advantages, is to assemble TECs *in vitro* [7].

The Kashlev laboratory has developed and optimized a number of strategies for preparation of TECs by combining purified S.c. Pol II or E.c. RNAP with a DNA template and short complimentary RNA primer (7–9 nucleotides long) [7,33,34]. The non-template DNA strand is then added to form a TEC that is capable of efficient and rapid elongation. Construction of TECs *in vitro* allows many modifications to be introduced into nucleic acids, potentially altering elongation in useful ways. Below we describe several modifications of the original assembly method improving and speeding up the pre-steady state kinetic analysis of Pol II/RNAP enzymes. We introduced an additional improvement to the standard pre-steady state protocol enabling rapid purification of the fully functional Pol II core using immobilization of hexahistidine-tagged S.c. Pol II (the tag is located in the Rpb3 subunit) on Ni-NTA agarose beads directly from the crude cell extract [34].

### 3.5. Immobilization of TECs

#### 3.5.1. Advantages

Bead immobilization allows repeated isolation and purification of TECs. It is often convenient, therefore, to do assays of RNA

460 elongation immobilized on affinity particles. Beads (i.e., Promega  
461 Magnesphere) with a sufficiently small diameter can be used in  
462 the KinTek RQF instruments with few difficulties. Many immobiliza-  
463 tion strategies are possible. With polymerase chain reaction, bio-  
464 tin-linked DNA primers can be used to synthesize biotinylated DNA  
465 for immobilization on streptavidin-coupled beads. For instance,  
466 tagging the non-template DNA strand used in TEC assembly ensu-  
467 res that immobilized TECs have a non-template strand during kin-  
468 etic analysis. S.c. Pol II can be affinity-purified through biotin or  
469 poly-histidine tags [7,34].

470 Rate data have routinely been quantified as a percent of rele-  
471 vant transcripts within a particular gel lane. A quantitative recov-  
472 ery of the RNA from the immobilized TECs can be a problem  
473 leading to some variations in the total amount of the labeled  
474 RNA in each sample. However, because transcripts are quantified  
475 as a ratio, it has not been necessary to determine the precise yield  
476 of TECs in a particular sample or experiment, and differing efficien-  
477 cies in TEC purification, recovery, or gel sample loading do not  
478 noticeably affect the consistency of the kinetic analysis.

### 479 3.5.2. Immobilization via a biotin group in DNA

480 In the human system, C40 TECs have been purified from HeLa  
481 cell nuclei extract, removing protein, NTPs, and other contami-  
482 nants. Because of the very high processivity of the Pol II TEC, most

483 complexes are recovered using this approach. TECs can be washed  
484 with high salt buffers and/or sarkosyl detergent, without notice-  
485 ably affecting their stability or response to addition of several elon-  
486 gation factors. Buffer-washed, salt-washed, and sarkosyl-washed  
487 TECs have very similar behavior in elongation (32 and data not  
488 shown). Sometimes, it is valuable to “walk” TECs immobilized on  
489 beads to a downstream sequence, which may involve repeated  
490 additions of NTPs that may require removal for the final reaction  
491 design. When EDTA is used as the reaction quenching agent, TECs  
492 do not dissociate from beads, so RNA can be recovered without  
493 ethanol precipitation for analysis on gels.

### 494 3.5.3. Immobilization of the TEC via protein tags

495 In control experiments, affinity tags do not influence elongation  
496 rates in noticeable ways ([33] and data not shown). Elongation  
497 rates measured on and off beads are very similar, indicating that  
498 kinetic measurements can be made on or off beads. If TECs are  
499 immobilized through a hexahistidine tag for purification, imidazole  
500 can be added to remove complexes from beads at the final step  
501 for quench flow studies [7]. Of course, in this case, some imidazole  
502 remains in the reaction during elongation. The experiments shown  
503 in Figs. 3–8 utilized histidine-tagged TECs obtained on Ni-NTA  
504 agarose beads and eluted with imidazole (working concentra-  
505 tion < 20 mM) before loading to the RQF-3 apparatus.

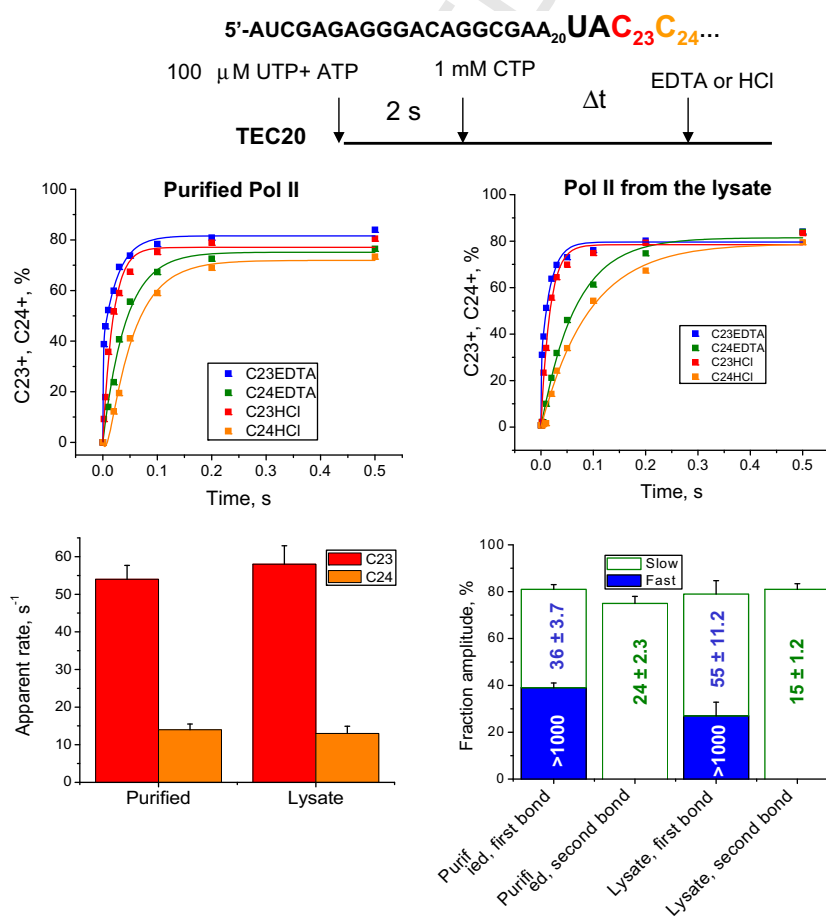


**Fig. 3.** TECs assembled from purified S.c. Pol II and S.c. Pol II pulled down from a lysate through a hexahistidine tag show similar elongation profiles. The reaction protocol and the RNA sequence are shown at the top of the figure. Numbers in the bottom right panel indicate apparent rates (units of s<sup>-1</sup>) determined by exponential curve fitting. Lower left panel, single exponential fits of the rate curves obtained with HCl quench are shown with standard error measurements from curve fitting. Lower right panel, double exponential curve fits of EDTA quench data. Double bars (filled blue and open green) indicate: fraction amplitudes; the corresponding rates (s<sup>-1</sup>) for the fractions are shown with numbers. Colors (red and orange: first and second bond, respectively, for HCl quench; blue and green: first and second bond, respectively, for EDTA quench) and errors (standard errors) are consistent in Figs. 3–7.

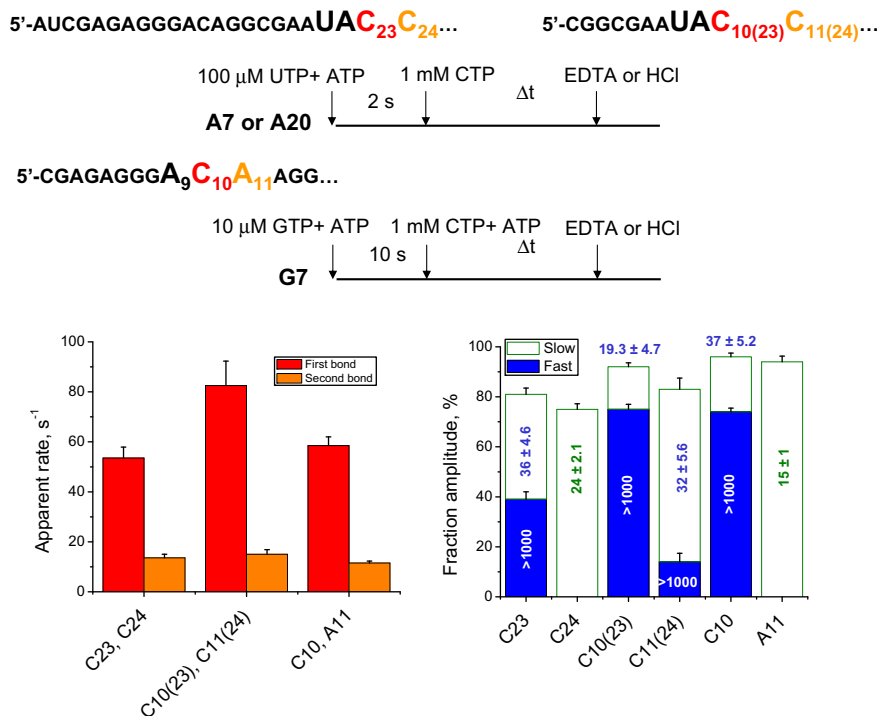


**Fig. 4.** Comparing elongation of S.c. Pol II TECs with different length RNAs and the same sequence or with the same length RNA and a different sequence. RNA sequences and protocols are at the top of the figure. C10(23), C11(24) indicates C10 and C11 transcripts in the same sequence context as the C23 and C24 transcripts. Left panel, HCl quench data. Right panel, EDTA quench data.

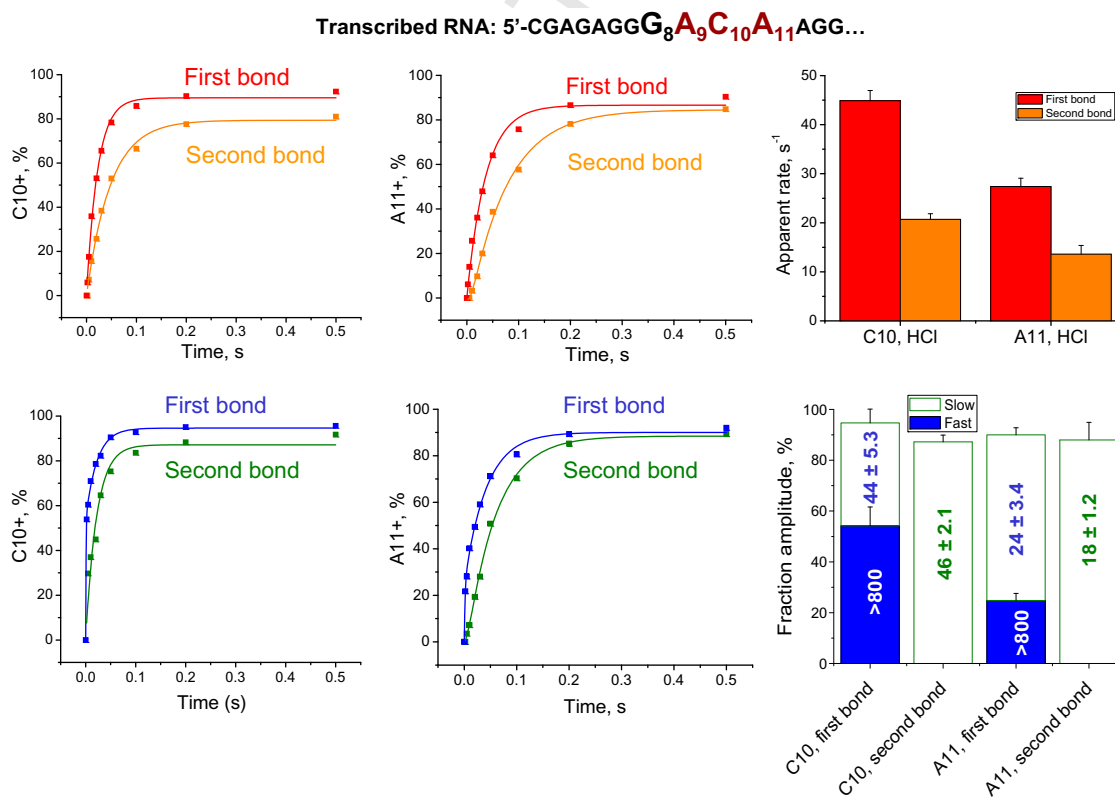


**Fig. 5.** C10 and A11 bonds are faster when they are synthesized as the first bond after a stall compared to the second bond. This result suggests a rate-limiting step during the processive transition between bonds. The sequence is shown at the top of the figure. Top panels, HCl quench data. Bottom panels, EDTA quench data.

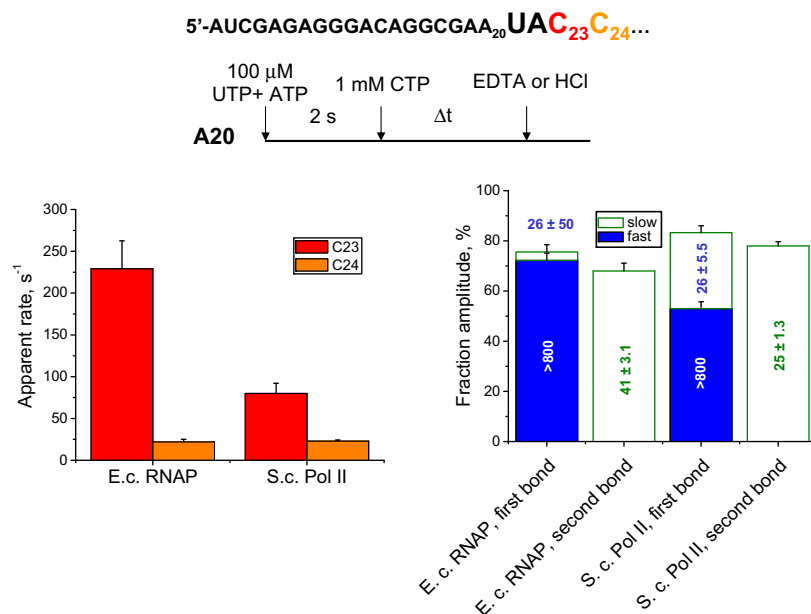


Fig. 6. Comparison of E.c. RNAP and S.c. Pol II TECs assembled from RNA and DNA oligonucleotides and formed on an identical sequence.

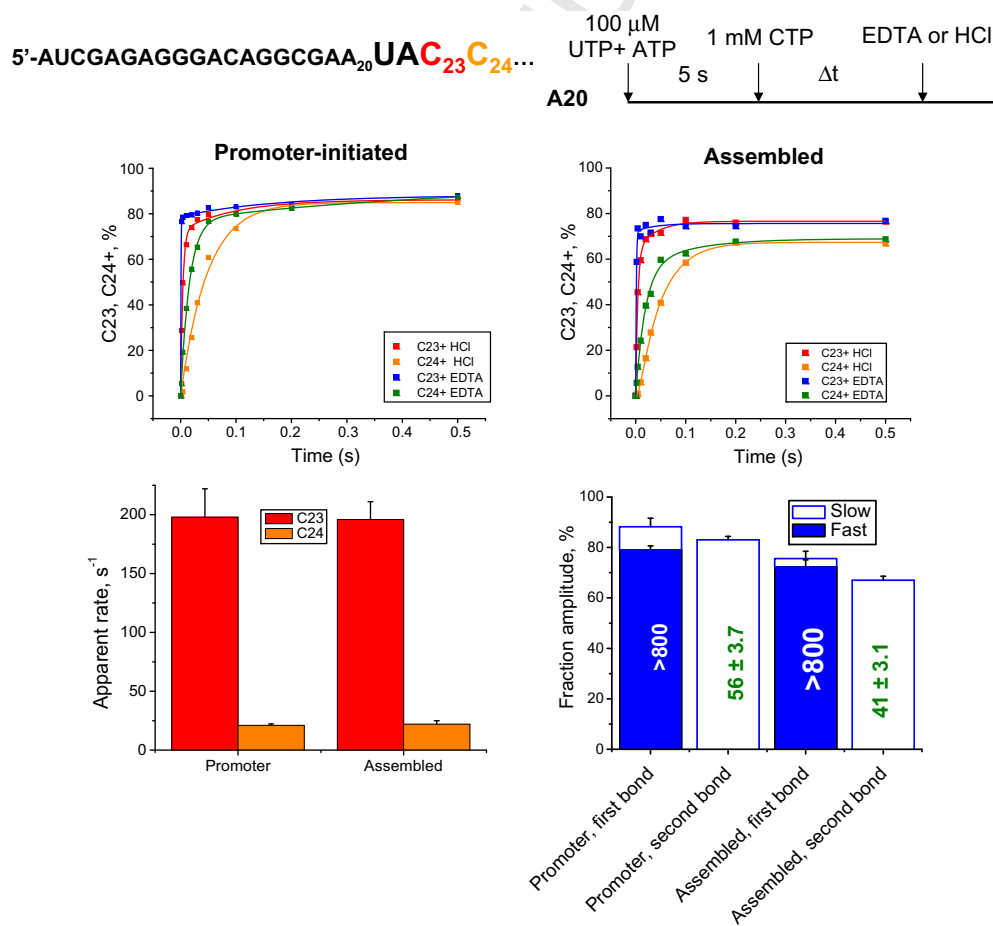
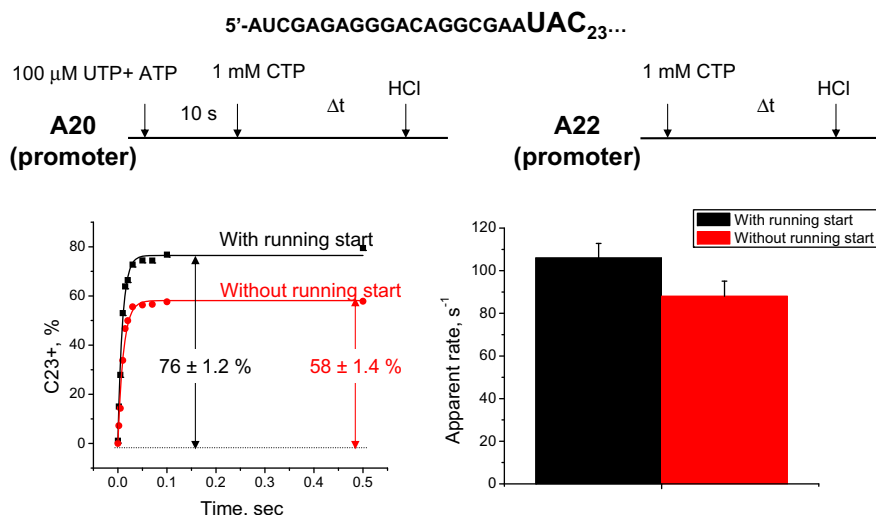


Fig. 7. Comparison of promoter initiated and assembled E.c. RNAP TECs.



**Fig. 8.** The running start protocol increases the fraction of promoter-initiated E.c. RNAP TECs on the active synthesis pathway. The protocol and sequence are shown at the top of the figure.

506 3.6. Comparison of transcription properties of purified *S.c. Pol II* core,  
507 and *S.c. Pol II* pulled down using histidine-tagged *Rpb3* from the whole  
508 cell lysate

509 Experiments with H.s. Pol II were performed with the enzyme  
510 pulled down from the nuclear extract followed by wash of the  
511 DNA-immobilized promoter-initiated TEC with sarkosyl [8–13].  
512 The exact protein composition of H.s. Pol II TECs has not been  
513 determined. With *S.c. Pol II*, we tested whether the pre-steady state  
514 characteristics of the TEC obtained by single-step purification were  
515 similar to those obtained with highly purified enzyme (Fig. 3). In  
516 contrast to immobilization of the H.s. Pol II TEC through DNA, we  
517 immobilized *S.c. Pol II* through a hexahistidine tag in the protein.  
518 For that purpose, TECs were assembled with the 5'-end labeled  
519 RNA9 using purified *S.c. Pol II* immobilized on Ni<sup>2+</sup>-NTA agarose  
520 or *S.c. Pol II* pulled down from the whole cell lysate on Ni<sup>2+</sup>-NTA  
521 agarose [34]. TEC A20 was obtained by incubation of TEC9 with  
522 10 μM ATP + CTP + GTP. A20 was eluted from the Ni<sup>2+</sup>-NTA agarose  
523 beads by incubation with 100 mM imidazole, and diluted with  
524 transcription buffer to bring imidazole concentration below  
525 20 mM. The A20 TEC was treated as outlined in the scheme of  
526 the experiment shown on top of Fig. 3. The curves show double-  
527 exponential fits for the formation of C23 in EDTA quench, and single-  
528 exponential fits for the data obtained by HCl quench, and for  
529 C24, EDTA quench. The plot at left summarizes the apparent rates  
530 for phosphodiester bond formation (HCl quench). The plot at right  
531 shows amplitudes of the fast and slow fractions (filled and open  
532 bars) in the substrate sequestration dynamics (EDTA quench).  
533 Numbers in the bars show the rates (s<sup>-1</sup>), determined with EDTA  
534 quench. Fitting rate data to a double exponential curve yields  
535 two rates associated with two amplitudes indicating the fraction  
536 of TECs associated with a particular rate of elongation.

537 No significant difference in the properties of the two Pol II pre-  
538 parations is observed. A characteristic “burst” in the reaction  
539 stopped by EDTA and a delay between the first and second bond  
540 formation are observed with both purified Pol II and Pol II pulled  
541 down from the lysate. Therefore, the main features of elongation  
542 by H.s. Pol II, reported for the TEC formed by promoter initiation  
543 from nuclear extracts (Fig. 1), and containing elongation factors  
544 TFIIF and TFIIS, are essentially the same as the characteristics of  
545 purified *S.c. Pol II* core enzyme (compare Figs. 1 and 3). Similar  
546 results were obtained with E.c. RNAP carrying a hexahistidine tag  
547 at the carboxy-terminus of the β' subunit (see below).

548 We should note here, that the presence of the “burst” fraction,  
549 which reflects rapid binding of the NTP-Mg<sup>2+</sup> substrate to the  
550 TEC and its commitment to phosphodiester bond formation, is  
551 not an intrinsic property of all *S.c. Pol II* and E.c. RNAP TECs. We  
552 found that the magnitude of the “burst” varied in a broad range  
553 among TECs transcribing different sequences and containing tran-  
554 scripts of different lengths (see below). Some E.c. RNAP TECs  
555 showed no detectable “burst” (data not shown), suggesting that  
556 rapid and stable sequestration of the incoming NTP-Mg<sup>2+</sup> may be  
557 sequence-specific. An absence of the burst in EDTA quench was  
558 recently reported for E.c. RNAP [31]; however, that observation  
559 was done at 50 μM concentration of NTP substrate, which likely  
560 is not sufficient to observe a burst of stable NTP-Mg<sup>2+</sup> loading in  
561 most of the TECs formed by any of the multi-subunit RNAPs [32].

562 3.7. Effect of transcript length and local sequence context on *S.c. Pol II*  
563 TECs

564 It has been reported that the full escape of mammalian Pol II  
565 from a promoter occurs at the 20–40-nt length of the nascent tran-  
566 script and the length of the RNA *per se* was crucial for escape [35].  
567 This result implied that the length of the transcript could affect cat-  
568 alytic properties of the enzyme. All of our conclusions with H.s. Pol  
569 II were made based on analysis of TECs with similar lengths of  
570 RNAs (40–50 nts). In this section, we compared the catalytic prop-  
571 erties of *S.c. Pol II* TECs with transcripts of different lengths but of  
572 the same 3'-terminal sequence (Fig. 4). This experiment addressed  
573 whether the length of the RNA would affect formation of the first  
574 bond and the processive transition to the second bond in a TEC  
575 transcribing the identical local DNA sequence. TECs G9, A7, and  
576 G7 were assembled with RNA9 (5'-AUCGAGAGG-3'), RNA7(20)  
577 (5'-CGGCGAA-3'), or RNA7 (5'-CGAGAGG-3'). The G9 TEC was  
578 incubated with 10 μM ATP + CTP + GTP to form A20. Note that A20  
579 and G7(20) have identical 3'-ends of the transcripts (Fig. 4). The  
580 running start and chase reactions were done as depicted in the  
581 reaction schemes. The apparent rates for phosphodiester bond  
582 formation (HCl quench) for the escape from the stall (first bond)  
583 and processive synthesis (second bond) are shown at the left.  
584 The plot at right shows the dynamics of the substrate sequestration  
585 (EDTA quench). The numbers show the apparent rates. The ampli-  
586 tudes of the fast and slow fractions are depicted by the filled bars  
587 and open bars, respectively. The DNA sequence for the assembly  
588 was (non-template strand) 5'-CCT ATA GGA TAC TTA CAG CCA

UCG AGA GGG ACA CGG CGA ATA CCC ATC CCA ATC GGC CTG CTG  
GT-3'. The sequences corresponding to RNA9 and RNA7(20) used  
 for the assembly are underlined. This experiment yielded the fol-  
 lowing conclusions:

- The TEC containing the short (9 nt) RNA sequesters the substrate more efficiently (has a higher “burst”) than the TEC formed in the same sequence context, but containing a 22-nt RNA of the identical 3'-proximal sequence.
- The increased sequestration of substrate correlates with and increases the apparent rate of first bond formation.
- Rapid sequestration of substrate NTP and delay in the second bond formation are observed in two different sequence contexts indicating a general nature of this phenomenon.

### 3.8. Analyses of the processive transition of the S.c. Pol II TEC

In this section, we confirmed the observation initially made with H.s. Pol II that the rate of NTP incorporation during escape from the stall (first bond) is higher than the rate of the same NTP incorporation during processive synthesis (second bond). In principle, but for the 25-ms lag in G45 appearance, the previously observed delay in the second bond formation could be caused by an intrinsically slower rate of the corresponding NTP incorporation (G44 (first bond) versus G45 (second bond) addition in the experiment of Fig. 1). The experiment shown in Fig. 5 distinguishes the delay caused during the processive transition, such as reverse isomerization, pyrophosphate release or translocation, from the apparent delay appearing because of a particular sequence context (a rapid bond followed by a slow bond). In the S.c. Pol II TEC we compared rates of incorporation of CTP to the +10 position as the first and the second bonds. The same experiment was done with incorporation of ATP to the +11 position of the transcript. For that purpose, transcription was started from G8 (C10, second bond), A9 (C10, first bond, and A11, second bond) or C10 (A11, first bond) by addition of 200  $\mu$ M ATP + CTP followed by stop of the reaction with HCl or EDTA. The rates for the first and second bond formations (HCl quench) are shown in the top right plot of Fig. 5. The dynamics of substrate sequestration (EDTA quench) is shown at the bottom right: the numbers show the apparent rates, and filled and open bars show the amplitudes of the fast and slow fractions. We concluded that:

- For the two separate template positions that we analyzed, the rate of the second bond was consistently slower than that of the first bond. This result indicated that the processive transition between the bonds, but not the local sequence context or chemical nature of the incoming NTP, represents a rate-limiting step during elongation.
- The amplitude of the “burst” fraction (sequestration of NTP) significantly varied between two adjacent template positions during formation of the first bond, further indicating the sequence specificity of this phenomenon.
- We note that the slow rates in EDTA quench were similar for the first and second bonds and the second bond rates in HCl quench were two times slower than the first bond rates.

### 3.9. E.c. RNAP and S.c. Pol II TECs compared within an identical sequence context

Pre-steady-state analyses of transcription elongation by E.c. RNAP were largely limited to analyses of a single bond formation

in a reaction stopped with EDTA [5,6]. The result of the experiment shown in Fig. 6 suggests that the dynamics of transcription elongation by E.c. RNAP and S.c. Pol II using the RTD protocol are fundamentally similar. The assembly method allows placement of different RNAPs in the same sequence context enabling a direct comparison of their catalytic mechanisms. Fig. 6 shows the EDTA and HCl quench data of C23 and C24 bond formation in the S.c. Pol II and E.c. RNAP TECs containing the same sequences of the DNA and nascent RNA. Briefly, E.c. RNAP and S.c. Pol II A20 TECs were obtained as described for the experiment shown in Fig. 4. The apparent rates of C23 and C24 bond formation (HCl quench) are shown in the plot at left (Fig. 6). Note a dramatic difference between the rates for the first and second bonds, suggesting that the processive transition (translocation with pyrophosphate release) was rate-limiting as described in Fig. 5. The dynamics of substrate sequestration (EDTA quench) is shown at right (Fig. 6). Filled and open bars depict the amplitudes of the fast and slow fractions, and the numbers show apparent rates for each fraction. We observed that E.c. RNAP formed the C23 bond faster, and sequestered CTP-Mg<sup>2+</sup> for both C23 and C24 more efficiently than S.c. Pol II. Characterization of additional TECs will be necessary to determine whether enhanced NTP sequestration is an intrinsic property of E.c. RNAP.

Otherwise both enzymes showed a remarkable similarity in the major catalytic characteristics of the first and the second bond formation that included (i) the presence of the 2-ms burst for first bond formation in the reaction quenched with EDTA, (ii) the uniform single-exponential rate of the first bond formation in the reaction quenched with HCl, and (iii) a substantial delay between the first and the second bond. These results indicate that E.c. RNAP and S.c. Pol II share the same two-step mechanism involving rapid binding of NTP and isomerization of the TEC into the catalytically competent state prior to bond formation. Based on a time gap between the first and second bonds, the processive transition between the two bonds is likely to be a rate-limiting step for E.c. RNAP, S.c. Pol II, and H.s. Pol II (Figs. 1 and 6).

### 3.10. Promoter-initiated and assembled E.c. RNAP TECs exhibit similar pre-steady state properties

Despite similarities between elongation profiles of promoter-initiated H.s. Pol II TECs and assembled TECs formed by S.c. Pol II and E.c. RNAP, a possibility remained that the observed characteristics of the latter two RNAPs reflect the peculiarities of the assembled TECs, rather than the true properties of S.c. Pol II and E.c. RNAP. To address this issue, catalytic properties of the promoter-initiated and assembled E.c. TECs were compared in an identical sequence context (Fig. 7). TECs carrying the same RNA transcript were obtained by: initiation from the bacteriophage T7 A1 promoter; or by assembly on a synthetic scaffold. The A1 promoter-initiated TEC20 was formed on a 156-bp DNA fragment after incubation of E.c. RNAP holoenzyme with ApUpC RNA primer and 250  $\mu$ M ATP + GTP (TEC11) followed by RNA labeling with  $\alpha$ -<sup>32</sup>P-CTP to form TEC12. TEC12 was chased to TEC20 (promoter A20) by 5 min incubation with 10  $\mu$ M ATP + CTP + GTP and the non-incorporated NTPs were removed by washing. The *in vitro* assembled counterpart of TEC20 was obtained as follows. TEC9 was assembled on a pair of 60-nt DNA oligonucleotides coding for the –20 to +40 segment of the A1 promoter and a 9-nt RNA primer (G9), labeled with  $\alpha$ -<sup>32</sup>P-CTP at the +12 position, followed by addition of 10  $\mu$ M ATP + CTP + GTP to elongate the RNA to 20-nt (assembled A20). For pre-steady-state analyses, both TECs were purified and subjected to a running start with 100  $\mu$ M UTP and ATP followed by addition of 1 mM CTP and quenched with EDTA



#### 4.4. Recombinant human elongation factors

RAP30 and RAP74 subunits were produced in bacterial cells, purified, and reconstituted into the transcription factor IIF (TFIIF) complex, as described [41,42]. Recombinant TFIIF (10 pmol) was used per 10  $\mu$ l reaction. TFIIS was produced from a pET expression vector and isolated by phosphocellulose and Mono-S chromatography. TFIIS (3 pmol) was used per 10  $\mu$ l reaction. Hepatitis delta antigen was prepared as described [25]. Hepatitis delta antigen (77 pmol) was added per 10  $\mu$ l reaction. These quantities of elongation factors were found to be functionally saturating for transcription stimulation activity (TFIIF and hepatitis delta antigen) and RNA cleavage (TFIIS).

#### 4.5. *S.c. Pol II* and *E.c. RNAP* TECs: assembly from DNA and RNA oligonucleotides

One to 10 pmol of RNAP is mixed with 2–20 pmol of RNA primer hybridized to the template DNA strand oligonucleotide (two-fold molar excess over RNAP) in 10–100  $\mu$ l of transcription buffer. The RNAP may be immobilized on beads or remain in solution. After 10 min incubation at room temperature (preferably with constant shaking at 800–1000 rpm), the non-template DNA strand (two- to fivefold molar excess over the RNA–DNA hybrid) is added to the assembly reaction, and the incubation continues for another 10 min. Subsequently, the TEC may be immobilized via an affinity tag on the protein or on the DNA, and the excess of RNA and DNA oligonucleotides is removed by washing with transcription buffer. The TEC immobilized on Ni–NTA agarose beads is eluted from the beads by addition of BSA to 0.2 mg/ml final concentration, and 1 M imidazole (pH 7.0) to 100 mM final concentration. The eluted TEC is separated from the beads by filtration through a 0.22 or 0.45  $\mu$ m membrane (Ultrafree-MC filter unit, Millipore, Billerica, MA) and diluted with transcription buffer. Assembly does not require immobilization of the TEC, and can be done with unmodified RNAP and oligonucleotides. In this case, the TEC may be purified from excess RNA and DNA by ultrafiltration through a 100-kDa cutoff membrane (Microcon YM-100, Millipore, Billerica, MA) by concentrating the sample after assembly, diluting it with 300  $\mu$ l transcription buffer, and concentrating it again to 10–15  $\mu$ l. Further details of the assembly protocol, including assembly of the TEC with *S.c. Pol II* pulled down from the whole cell extract, can be found in [33,34].

#### 4.6. *E.c. RNAP* TEC: T7 A1 promoter-based initiation

One to 2 pmol of 156-bp template DNA are combined with 1–2 pmol of *E.c. RNAP* in 5  $\mu$ l transcription buffer and incubated for 5 min at 37  $^{\circ}$ C to form an open complex. ApUpC primer is added to the open complex to achieve 100  $\mu$ M final concentration, ATP and GTP are added to achieve 250  $\mu$ M final concentration, and TEC11 is formed by 5 min incubation at 37  $^{\circ}$ C. Subsequently, TEC11 is immobilized on Ni–NTA agarose beads, washed with transcription buffer and transcription buffer containing 1 M KCl, and labeled by a 5 min incubation with 0.3  $\mu$ M  $\alpha$ - $^{32}$ P CTP (800 Ci/mmol, Perkin Elmer, Waltham, MA) to form TEC12.

#### 4.7. RTD protocol

The RQF-3 instrument is set up with transcription buffer in the left and right syringes and quench solution (1 M HCl or 0.5 M EDTA (pH 7)) in the middle syringe. Fifteen microliters NTP substrate for elongation is loaded at twice its working concentration in the right sample loop and the valves are moved to the “fire” position.

In the running start, ATP is added to C40 TECs to advance to the A41, A42, and A43 positions. The concentration of ATP used and the

time of incubation were optimized to maximize synthesis of A43 and to minimize misincorporation of AMP for GMP at G44. Depending on the protocol, ATP additions (10 or 100  $\mu$ M) were for 30 (TFIIF + TFIIS), 60 (HDAG), or 120 s (no elongation factors, defective TFIIF mutants). CTP and UTP 1–20  $\mu$ M may be added to maximize the yield of A43. During ATP incubation the sample is loaded in the left sample loop (15  $\mu$ l volume) of the RQF-3 instrument and the valve set to the “fire” position. At the end of the ATP incubation period, the rapid mixing program is initiated, and the sample collected. Equal volume mixing of reagents between the left and right sample loops is assumed to give working concentrations of reagents.

For EDTA quenched samples, TECs remain intact, and the RNA can be collected on metal beads with a magnet to remove the supernatant. When the off bead supernatant is examined on gels, no free RNA is detected. The sample on beads can then be boiled in gel loading buffer in preparation for electrophoresis. Using this approach, all RNAs are recovered at the same efficiency. When the kinetic measurements were performed using TECs in solution, the samples (150–200  $\mu$ l) were collected in reaction tubes each containing 2  $\mu$ l of 20 mg/ml oyster glycogen (Type II, Sigma G8751), dissolved in water and passed through 0.22  $\mu$ m filter. The samples were precipitated by addition of 100  $\mu$ l 2 M Tris–HCl (pH 9.0), 30  $\mu$ l 3 M sodium acetate (pH 7.0), and 1 ml of ethanol. Addition of Tris–HCl (pH 9.0) and adjusting the sodium acetate pH to 7.0 is essential to ensure that EDTA does not precipitate upon ethanol addition.

For HCl quenched samples, the sample collection tube contains sufficient Tris–base solution to neutralize the sample (determined empirically), so that the RNA is not maintained for a long period at low pH. Because HCl quenching dissociates RNA, beads are discarded, and the supernatant is ethanol precipitated and resuspended in gel loading buffer for electrophoresis. When non-immobilized TECs were used, the samples were collected in the tubes containing 2  $\mu$ l of 20 mg/ml oyster glycogen, 150  $\mu$ l 2 M Tris–HCl (pH 9.0), and 30  $\mu$ l 3 M sodium acetate (pH 7.0). One milliliter of ethanol was added to precipitate the RNA. We find that RNAs 40 nucleotides and longer are efficiently recovered for electrophoresis. Smaller RNAs of different lengths may not be recovered by ethanol precipitation at identical efficiencies; addition of glycogen, however, promotes efficient precipitation of even very short (7-nt) RNAs.

#### 4.8. Electrophoresis

Samples are electrophoresed in 1 $\times$  Tris–borate–EDTA buffer. Gels to resolve 40–50 nt RNAs are typically 14% acrylamide, with 20:1 ratio acrylamide:bis-acrylamide for C40–G45 complexes, and contain 50% w/v urea. The shorter (7–25 nt) RNAs were resolved in 20% (19:1 acrylamide:bis-acrylamide) gels containing 1 $\times$  TBE and 7 M urea.

#### 4.9. Phosphorimager quantification of gels

We currently use a General Electric STORM820 and TYPHOON 9200 (General Electric) phosphorimagers for quantification of gel bands. Relevant bands are quantified and normalized as 100% of signal using ImageQuant software. In this way, a correction is made for uneven sample recovery and gel loading (see Fig. 1).

## 5. Modeling

Quench flow studies provide the timing of stable NTP–Mg $^{2+}$  loading and phosphodiester bond synthesis through formation of multiple bonds. With related stop-flow technology, Johnson et al.

947 have determined the kinetics of pyrophosphate release for E.c.  
948 RNAP, using pyrophosphatase to cleave released pyrophosphate  
949 and a fluorescent phosphate trap for detection [32]. They found  
950 that pyrophosphate release was dependent on templated loading  
951 of the next NTP substrate, consistent with NTPs pairing to template  
952 in the pre-translocated TEC and being carried into the active site  
953 upon translocation, as pyrophosphate is released. Non-templated  
954 NTPs did not stimulate pyrophosphate release. Putting quench  
955 flow and stop flow techniques together, therefore, would provide  
956 three “signposts”, NTP-Mg<sup>2+</sup> sequestration, bond synthesis, and  
957 pyrophosphate release, for each RNAP bond formation.

958 One goal has been to use kinetic modeling to simulate the mul-  
959 ti-subunit RNAP reaction mechanism through formation of at least  
960 two phosphodiester bonds, specifying rate-limiting and other de-  
961 tected steps. This seemingly simple goal has provoked a great deal  
962 of controversy and a large number of models. Erie and co-workers  
963 proposed an allosteric model for elongation [2,5,6]. Burton and co-  
964 workers proposed an NTP-driven translocation model [4,8-  
965 11,13,43]. Nudler, Ruckenstein, and co-workers proposed a dual  
966 ratchet mechanism [16].

967 Kashlev, Burton, and colleagues have attempted to reduce the  
968 complexity of the mechanism to a linear, reversible isomerization  
969 model, but this model has only so far been applied to formation  
970 of a single phosphodiester bond [7]. The difficulty with single  
971 bond analysis is that it neglects the processive transition between  
972 bonds, which is a rate-limiting step. Which model will ultimately  
973 best describe the elongation mechanism we are not currently cer-  
974 tain, but this effort continues. Modeling has been done with pro-  
975 grams DYNAFIT [44], KinTek Global Kinetic Explorer (KinTek  
976 Corporation, Austin, TX), and MatLab. We find that current ver-  
977 sions of KinTek Global Kinetic Explorer lack features to model  
978 EDTA quench data in the most useful fashion. Because the reac-  
979 tion does not stop upon EDTA addition, EDTA quench data should  
980 be modeled as if it were pulse-chase data. In a pulse-chase strat-  
981 egy, an excess of an unlabeled NTP would be added to cause dilu-  
982 tion of a previously added radioactive NTP. EDTA addition  
983 depletes free NTP-Mg<sup>2+</sup> without affecting enzyme-bound NTP-  
984 Mg<sup>2+</sup>. Another problem with EDTA quenching is that, in some  
985 reaction schemes, addition of EDTA is consequential. That is to  
986 say that EDTA acts as a component of the reaction, by removing  
987 Mg<sup>2+</sup>. The Burton laboratory has shown evidence that EDTA can  
988 result in isomerization reversal and phosphodiester bond reversal,  
989 indicating that there is a role for Mg<sup>2+</sup> in the stable completion of  
990 a phosphodiester bond after phosphodiester bond synthesis  
991 (Fig. 2). The KinTek program does not have features to handle  
992 EDTA quench data sets as pulse-chase reactions or to use the  
993 EDTA quencher as a chemical component of the reaction.

## 994 Acknowledgments

995 This work was in part supported by the National Institutes of  
996 Health Grant GM57461 (to Z.F.B.). Z.F.B. receives support from  
997 Michigan State University, the Michigan State University Agricul-  
998 tural Experiment Station, and the Michigan State University Col-  
999 lege of Osteopathic Medicine. The contents of this publication do

not necessarily reveal the views or policies of the Department of  
Health and Human Services, nor does mention of trade names,  
commercial products, or organizations imply endorsement by the  
U.S. Government.

## References

- [1] K.M. Herbert, W.J. Greenleaf, S.M. Block, *Annu. Rev. Biochem.* 77 (2008) 149–176.
- [2] J.E. Foster, S.F. Holmes, D.A. Erie, *Cell* 106 (2001) 243–252.
- [3] X.Q. Gong, Y.A. Nedialkov, Z.F. Burton, *J. Biol. Chem.* 279 (2004) 27422–27427.
- [4] X.Q. Gong, C. Zhang, M. Feig, Z.F. Burton, *Mol. Cell* 18 (2005) 461–470.
- [5] S.F. Holmes, J.E. Foster, D.A. Erie, *Methods Enzymol.* 371 (2003) 71–81.
- [6] S.F. Holmes, T.J. Santangelo, C.K. Cunningham, J.W. Roberts, D.A. Erie, *J. Biol. Chem.* 281 (2006) 18677–18683.
- [7] M.L. Kireeva, Y.A. Nedialkov, G.H. Cremona, Y.A. Purto, L. Lubkowska, F. Malagon, Z.F. Burton, J.N. Strathern, M. Kashlev, *Mol. Cell* (2008).
- [8] Y.A. Nedialkov, X.Q. Gong, S.L. Hovde, Y. Yamaguchi, H. Handa, J.H. Geiger, H. Yan, Z.F. Burton, *J. Biol. Chem.* 278 (2003) 18303–18312.
- [9] Y.A. Nedialkov, X.Q. Gong, Y. Yamaguchi, H. Handa, Z.F. Burton, *Methods Enzymol.* 371 (2003) 252–264.
- [10] Y. Xiong, Z.F. Burton, *J. Biol. Chem.* 282 (2007) 36582–36592.
- [11] C. Zhang, Z.F. Burton, *J. Mol. Biol.* 342 (2004) 1085–1099.
- [12] C. Zhang, H. Yan, Z.F. Burton, *J. Biol. Chem.* 278 (2003) 50101–50111.
- [13] C. Zhang, K.L. Zobeck, Z.F. Burton, *Mol. Cell. Biol.* 25 (2005) 3583–3595.
- [14] S.S. Patel, I. Wong, K.A. Johnson, *Biochemistry* 30 (1991) 511–525.
- [15] K.A. Johnson, *Methods Enzymol.* 249 (1995) 38–61.
- [16] G. Bar-Nahum, V. Epshtein, A.E. Ruckenstein, R. Rafikov, A. Mustaev, E. Nudler, *Cell* 120 (2005) 183–193.
- [17] M.G. Izban, D.S. Luse, *J. Biol. Chem.* 268 (1993) 12874–12885.
- [18] M.D. Rudd, M.G. Izban, D.S. Luse, *Proc. Natl. Acad. Sci. USA* 91 (1994) 8057–8061.
- [19] N. Komissarova, M. Kashlev, *Proc. Natl. Acad. Sci. USA* 94 (1997) 1755–1760.
- [20] N. Komissarova, M. Kashlev, *J. Biol. Chem.* 272 (1997) 15329–15338.
- [21] J.J. Arnold, C.E. Cameron, *Biochemistry* 43 (2004) 5126–5137.
- [22] J.J. Arnold, D.W. Gohara, C.E. Cameron, *Biochemistry* 43 (2004) 5138–5148.
- [23] N.N. Batada, K.D. Westover, D.A. Bushnell, M. Levitt, R.D. Kornberg, *Proc. Natl. Acad. Sci. USA* 101 (2004) 17361–17364.
- [24] Y. Yamaguchi, S. Delehouzee, H. Handa, *Microbes Infect.* 4 (2002) 1169–1175.
- [25] Y. Yamaguchi, J. Filipovska, K. Yano, A. Furuya, N. Inukai, T. Narita, T. Wada, S. Sugimoto, M.M. Konarska, H. Handa, *Science* 293 (2001) 124–127.
- [26] Y. Yamaguchi, T. Mura, S. Chanarat, S. Okamoto, H. Handa, *Genes Cells* 12 (2007) 863–875.
- [27] F. Brueckner, P. Cramer, *Nat. Struct. Mol. Biol.* 15 (2008) 811–818.
- [28] D.A. Bushnell, P. Cramer, R.D. Kornberg, *Proc. Natl. Acad. Sci. USA* 99 (2002) 1218–1222.
- [29] D. Wang, D.A. Bushnell, K.D. Westover, C.D. Kaplan, R.D. Kornberg, *Cell* 127 (2006) 941–954.
- [30] D.R. Chafin, H. Guo, D.H. Price, *J. Biol. Chem.* 270 (1995) 19114–19119.
- [31] M.D. Rudd, D.S. Luse, *J. Biol. Chem.* 271 (1996) 21549–21558.
- [32] R.S. Johnson, M. Strausbauch, R. Cooper, J.K. Register, *J. Mol. Biol.* 381 (2008) 1106–1113.
- [33] M.L. Kireeva, N. Komissarova, D.S. Waugh, M. Kashlev, *J. Biol. Chem.* 275 (2000) 6530–6536.
- [34] M.L. Kireeva, L. Lubkowska, N. Komissarova, M. Kashlev, *Methods Enzymol.* 370 (2003) 138–155.
- [35] M. Pal, D. McKean, D.S. Luse, *Mol. Cell. Biol.* 21 (2001) 5815–5825.
- [36] J.D. Funk, Y.A. Nedialkov, D. Xu, Z.F. Burton, *J. Biol. Chem.* 277 (2002) 46998–47003.
- [37] I. Samkurashvili, D.S. Luse, *J. Biol. Chem.* 271 (1996) 23495–23505.
- [38] D.J. Shapiro, P.A. Sharp, W.W. Wahli, M.J. Keller, *DNA* 7 (1988) 47–55.
- [39] T.E. Adamson, S.M. Shore, D.H. Price, *Methods Enzymol.* 371 (2003) 264–275.
- [40] B. Cheng, D.H. Price, *J. Biol. Chem.* 282 (2007) 21901–21912.
- [41] B.Q. Wang, C.F. Kostrub, A. Finkelstein, Z.F. Burton, *Protein Expr. Purif.* 4 (1993) 207–214.
- [42] B.Q. Wang, L. Lei, Z.F. Burton, *Protein Expr. Purif.* 5 (1994) 476–485.
- [43] Z.F. Burton, M. Feig, X.Q. Gong, C. Zhang, Y.A. Nedialkov, Y. Xiong, *Biochem. Cell Biol.* 83 (2005) 486–496.
- [44] P. Kuzmic, *Anal. Biochem.* 237 (1996) 260–273.